NANO LETTERS

2005
Vol. 5, No. 9
1809−1813

Femtosecond Spectroscopy of Carrier Relaxation Dynamics in Type II CdSe/CdTe Tetrapod Heteronanostructures

P. Peng, D. J. Milliron, S. M. Hughes, Justin C. Johnson,[†] A. Paul Alivisatos,[‡] and Richard J. Saykally*

Department of Chemistry, University of California, Berkeley, California 94720-1460

Received June 20, 2005; Revised Manuscript Received August 15, 2005

ABSTRACT

Branched nanocrystal heterostructures synthesized from CdSe and CdTe exhibit a type II band structure alignment that induces separation of charge upon photoexcitation and localizes carriers to different regions of the tetrahedral geometry. The dynamics of carrier relaxation examined with femtosecond pump–probe spectroscopy showed heterostructures having rise times and biexponential decays longer than those of nanorods with similar dimensions. This is attributed to weaker interactions with surface states and nonradiative relaxation channels afforded by the type II alignment.

Type II heteronanostructures displaying polytypism in the form of linear and branched tetrapods have recently been demonstrated,[1] just over a year after the first colloidal core/shell type II quantum dots (QD) were reported.[2] Figure 1 shows two different tetrapods, core/shell and rocket, both composed of CdSe ($E_g^{bulk} = 1.75$ eV at 300 K) and CdTe ($E_g^{bulk} = 1.48$ eV at 300 K). A rocket tetrapod comprises, conceptually, a CdTe tetrapod with a CdSe rod inserted between the core and one of the arms. In core/shell tetrapods, a CdSe shell encompasses a CdTe tetrapod. The interface (Figure 2) that is formed from the alignment of the band structures is such that the lowest conduction band states are in CdSe and lowest valence band states are in CdTe. Electrical and optical properties are not expected to be the same as those of nanorods and dots. Theoretical simulations have indeed predicted spatial distributions of electrons and holes to occur in different regions of single-component[3] and heterostructure tetrapods.[1] To date there have not been time-resolved, spectroscopic studies on tetrapods, and only recently have nanocrystals (NCs) possessing a type II heterointerface gained attention.[4−6] Yet these heterostructures are interesting because the formation of a new band gap at the interface may be utilized as either a radiative recombination center or a location where separation of charge can occur. Experiments on type II NCs have used fluorescence upconversion techniques to describe the rates at which carriers reach the interfacial band gap[4] or have varied growth conditions to produce changes in the photoluminescence and absorbance.[5,6] Optical hole burning and transient absorption studies have also been able to monitor the localization dynamics of separated charges in systems such as the CdS/HgS/CdS quantum dot quantum well.[7−9]

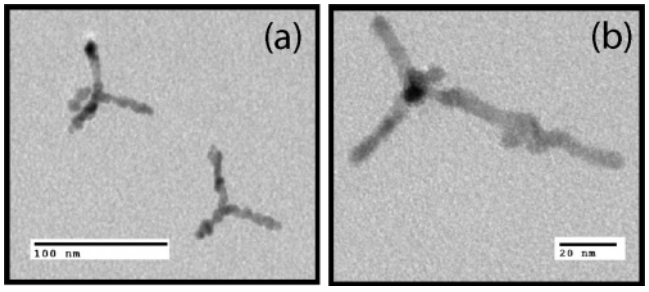

Figure 1. TEM images of the heterostructures studied include (a) core/shell tetrapods consisting of a CdSe shell encompassing a CdTe tetrapod and (b) rocket tetrapods comprising a CdTe tetrapod with a CdSe rod inserted between the core and one of the arms.

Potential applications of heteronanostructures that require fast time scales of operation will benefit from an understanding of the carrier dynamics. In photovoltaics for example, longer charge carrier, or recombination, lifetimes on the order of tens of picoseconds are desirable such that there is transfer of as much charge as possible.[10] Time-resolved experiments on nanostructures in the past decade have determined a multitude of factors that influence the kinetics of relaxation.[11,12] From the early model of a phonon bottleneck in

* Corresponding author: e-mail, saykally@uclink.berkeley.edu; office, 510 642-8269; fax, 510 642-8566.

[†] Present address: National Renewable Energy Laboratory, Golden, CO 80401.

[‡] Also at Materials Science Division, Lawrence Berkeley National Laboratory, Berkeley, CA 94720.

10.1021/nl0511667 CCC: $30.25
Published on Web 00/00/0000

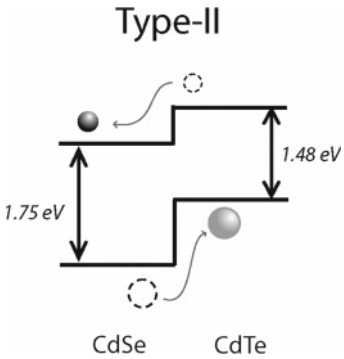

Figure 2. Separation of charges occurs at the type II interface formed by CdSe ($E_g^{bulk} = 1.75$ eV at 300 K) and CdTe ($E_g^{bulk} = 1.48$ eV at 300 K).

three-dimensionally quantum-confined quantum dots[13] to recent modifications of the theory that account for an electron−hole coupling mechanism[14] or interaction with the environment,[15] a consistent description of relaxation has been evolving. The effect of shape on the rate of relaxation was first reported by El-Sayed et al. in a comparison between nanorods and dots.[16] The slower electronic dynamics observed in rods was attributed to a surface mechanism that was more pronounced for the higher surface area dot. Nozik et al. further studied the dynamics of electron cooling in CdSe rods of different diameters and same lengths and found the relaxation to be faster in thinner rods.[17] Characterization of the tetrapods adds a new topology to the shape-dependent dynamics in the recent literature.[17,18] To study the carrier relaxation and indirectly observe the charge separation in the rocket and core/shell tetrapods (Figure 1), we conducted femtosecond pump−probe spectroscopy experiments using a 400 nm pump and a visible, near-IR (1.9 μm), or mid-IR (4.5 μm) probe. Visible probes interrogate the rates of relaxation of electrons while infrared probes provide complementary information about the relaxation of holes.

Variation in the ratio of surfactants along with control of temperature, concentration, and reactant ratios promote the nucleation and subsequent anisotropic growth of nanorods and dots, leading to formation of controllably branched colloidal nanostructures. Epitaxial growth of a second material to form a heterostructure can occur uniformly, as in core/shell structures, or selectively on the ends of nanorod sections to form a more complex heterostructure. Organic surfactants such as trialkylphosphines, trioctylphosphine oxide (TOPO), and alkylphosphonic acids cap the nanocrystals in solution and serve to passivate surface states and prevent oxidation. The synthesis of the materials investigated in this work has been described elsewhere.[1,19,20]

Rocket tetrapods are formed by first synthesizing CdSe rods, with a length of 49.76 ± 9.51 nm and diameter 6.36 ± 0.93 nm. Each end of the CdSe rods nucleates growth of CdTe—linear extension from one end and three symmetric branches from the other—so that the rod becomes embedded in the long arm of the rocket tetrapod. The diameter remains nearly unchanged (6.00 ± 0.85 nm), and this arm becomes 86.35 ± 9.22 nm upon growing the CdTe sections. For the core/shell tetrapods, a CdSe shell of varying uniformity is

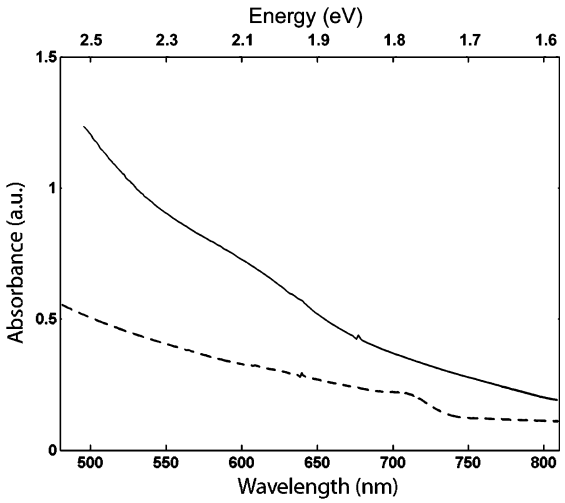

Figure 3. Absorbance spectra of the rocket (- - -) and core/shell (—) tetrapod heterostructures. The photoluminescence spectra[1] of both heterostructures are effectively quenched in the visible spectral region owing to the high degree of charge separation that occurs at the interface.

overgrown on a CdTe tetrapod of 39.44 ± 6.93 nm long arms and 5.71 ± 0.76 nm diameter, resulting in arms 39.06 ± 6.57 nm in length and 8.26 ± 1.12 nm in diameter. Transmission electron microscope (TEM) images of the two structures are shown in parts a and b of Figure 1. Absorbance spectra in Figure 3 show a resolvable first excitonic transition arising from CdTe for the rocket tetrapods, whereas the core/shell tetrapods have no resolvable peaks. Moreover, these spectra all possess longer low energy tails compared to CdSe rods or tetrapods, or CdTe tetrapods, suggesting the existence of spatially indirect transitions, lower in energy than the bulk band gap of either material, due to the type II band alignment.

A commercial regenerative/bowtie amplifier (1 kHz, Spectra-Physics, Spitfire), seeded by a home-built Ti:sapphire oscillator (88 MHz), produces 1.5 mJ, 100 fs pulses at a fundamental wavelength of 800 nm. A portion (4%) of this light is focused into a 2 mm sapphire plate to generate a white light continuum probe (450−900 nm) that is spatially filtered and selected for specific wavelengths using interference filters of ±5 nm. Another fraction (11%) is frequency-doubled (400 nm) in a β-barium borate (BBO) crystal. The remainder of the fundamental beam pumps an optical parametric amplifier (OPA, TOPAS, Quantronix), which produces wavelength-tunable pulses in the infrared. The 400 nm beam used to excite the heterostructures is chopped (Melles-Griot) optically at 500 Hz for lock-in detection and directed along a track capable of 50 fs step resolution over 2 ns of track length.

The pump and probe pulses are focused respectively to spot sizes of 500 and 250 μm on a 1.0 mm path length quartz cuvette (Spectrocell) that holds ca. 600 μL of the colloidal samples. Solutions of 0.5−1.2 optical densities at 500 nm are prepared under Ar immediately before each experiment, and neutral density filters maintain excitation powers at $\leq$1.0μJ/pulse just before reaching the sample. The formula developed by Yu et al. is used to find extinction coefficients and, in turn, an estimated number of particles in solution.[21]

Table 1. Summary of Exponential Fits from Visible and Infrared Probes of Rocket and Core/Shell Tetrapods

	rocket tetrapods		core/shell tetrapods	
probe wavelength	rise time	decay time(s)	rise time	decay time(s)
510 nm	380 fs	<150 fs 17.7 ± 5.4 ps	200 fs	6.72 ± 1.4 ps 47 ± 30 ps
band edge (700−725 nm)	2.1 ps	4.43 ± 1.8 ps 128 ± 23 ps	0.95 ps	2.57 ± 2.0 ps 9.0 ± 5.0 ps
1.9 μm	<150 fs	<150 fs 8.25 ± 0.4 ps	<150 fs	<150 fs 3.34 ± 0.4 ps
4.5 μm	<150 fs	5.75 ± 0.9 ps 62.8 ± 30 ps	<150 fs	6.71 ± 1.2 ps 35 ± 17 ps

The product of the number of pump photons incident per area (pump fluence, j) and the absorption cross section ($\sigma \sim 10^{-13}$ cm^2) gives an average excitation of electron−hole (e−h) pairs per particle, $\langle N_0 \rangle = j\sigma$, of 0.3−0.6. Less than one e−h pair excited with each pulse in solution avoids multiparticle processes such as nonradiative Auger recombination. Probe transmission is detected with either a mercury−cadmium−telluride detector (IR Associates) for infrared signals or else with a photodiode (Thor Labs). Boxcar integrators average the probe signals when pump excitation is present (T) and absent (T_0). Plots and best fits to differential transmission ($\Delta T/T$, where $\Delta T = T - T_0$) are carried out with MatLab. Care is taken to pump different spots on the cuvette or to keep excitation at a minimum, as prolonged focus at one location produces noticeable evidence of particle aggregation.

The difference in effective masses ($m_h/m_e \approx 6$) of the carriers in the heterostructures suggests a priori that electrons and holes do not relax with the same rate—lighter electrons are expected to cool at a slower rate. In support of this assumption, carrier-quenching experiments have demonstrated that probes in the visible region extract relaxation rates of electrons through conduction band states whereas IR probes yield hole dynamics.[16,18,22,23]

Table 1 summarizes the results.

When excited electrons relax into available states (state filling), the upper energy levels matching the visible probe are populated and the absorption bleaches. Recovery of absorption follows as depopulation from the excited energy levels and further relaxation of the electron to the band edge occurs. The time it takes to reach maximal transmission is the rise, or cooling, time of the electron. Probing energy levels from 2.44 eV (510 nm) to the band-edge reveals increasingly longer cooling times—lower states take longer to populate. Figure 4 depicts transient bleaching dynamics of an ensemble of core/shell tetrapods. The highest energy state probed is populated within ~200 fs while bleaching of the lowest state 1.78 eV (700 nm) takes 0.95 ps. Intermediate states, omitted for clarity, show an expected decrease in relaxation rate for lower energy probes. Rocket tetrapods (Table 1) take nearly twice as long to populate both the higher (380 fs) and lower (2.1 ps) levels. Most of the decays were fit optimally with biexponentials and possess a fast

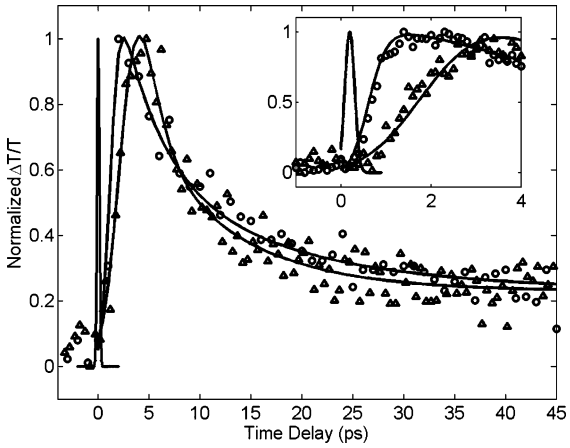

Figure 4. Electronic relaxation from higher energy (510 nm, 2.44 eV, ○) to lower, band-edge energy (700 nm, 1.78 eV, △) states in core/shell tetrapods. System response is superimposed at delay time zero. Inset: magnification of early times showing slower decay to lower energy level.

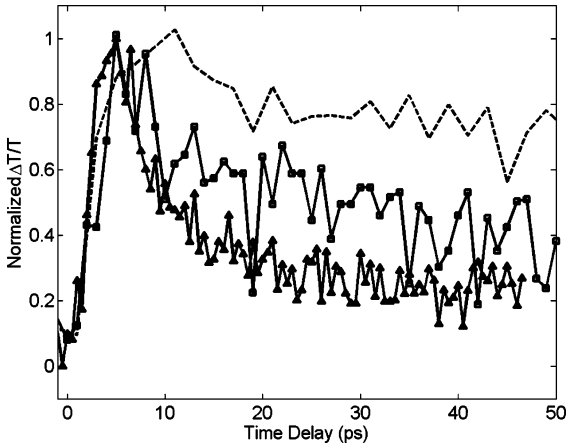

Figure 5. Pump (400 nm) and probe (725 or 700 nm) of excitonic states as indirect observation of charge separation in rocket (△) and core/shell (□) tetrapods, as compared to a CdSe rod (- - -) of comparable length and diameter.

picosecond component and a slightly longer (tens of picoseconds) second component.

Excitonic peaks visible in the absorption spectrum (Figure 3) are pumped at 400 nm and probed for the rate at which the $1S_{(e)} - 1S_{3/2(h)}$ level is populated. Figure 5 compares the rise of the exciton $1S_{(e)}$ bleach signal at 700 nm in core/shell and 725 nm in rocket tetrapods to that in CdSe rods of comparable length and diameter. The transmission in the CdSe rod decays slightly after 10 ps yet remains largely optically transparent for more than 50 ps. The transition in the heterostructures, however, begins to decay after 4 ps of maximal transmission because the more weakly interacting e−h pair dissociates.

The near-IR (0.65 eV) and mid-IR (260 meV) probes couple transitions between intraband states in the valence band, thereby providing information about the relaxation of holes. At higher energy, the near-IR probes transitions further from the band-edge than the mid-IR. Figure 6 depicts the absorption of the near-IR probe when holes are excited into the band and the subsequent recovery of transmission as holes

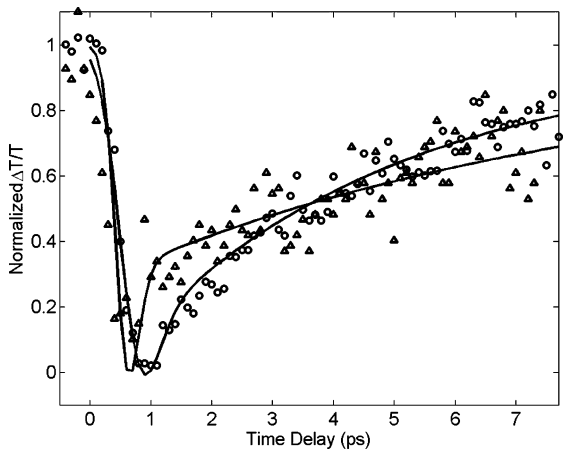

Figure 6. Near-IR traces of both tetrapods show an ultrafast decay component at short times but is faster in rockets (△) than in core/shells (○). At longer times, the two decay rates are comparable. (See Table 1.)

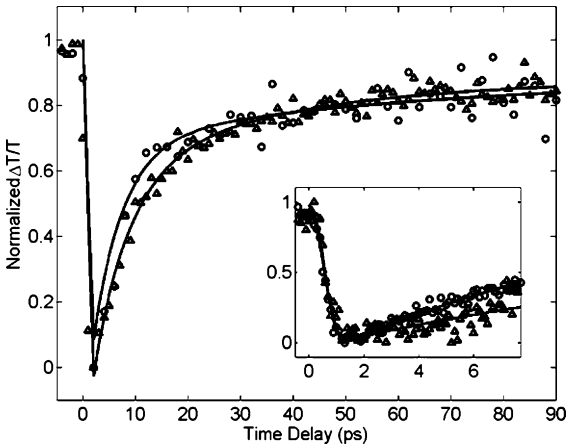

Figure 7. Mid-IR absorption and subsequent recovery of transmission in core/shells (○) and rockets (△) measures the charge carrier lifetime. Inset shows that there are no ultrafast components associated with the decay like that in the near-IR transients (Figure 6).

relax. Here, the rise time refers to the time it takes to reach zero transmission and is below the resolution of the probe pulse width (<150 fs)—in contrast to the picosecond rise times of electrons. By analogy, the recovery of transmission is the decay time constant listed in Table 1. The holes relax with an ultrafast component in both rockets and core/shells, with weighting factors in the fits of 0.27 and 0.15. At longer time delay, the two time constants (8.25 and 3.34 ps, respectively) are slower compared to CdSe nanoparticles with reported monoexponential lifetimes of 1.2[23] to 1.5 ps.[11] The mid-IR has an energy (260 meV) less than that of the near-IR and is close to intraband states at the valence band edge. It is therefore a measure of the hole carrier lifetime at long time delay as shown in Figure 7. Unlike the near-IR there are no ultrafast components in the decay times (inset of Figure 7). Hole relaxation in core/shells occurs with time constants of 5.75 and 62.8 ps; in rockets, relaxation occurs with time constants of 6.71 and 35 ps. Within the uncertainty of the fits, the kinetics of hole relaxation probed with mid-IR in the two heterostructures are comparable.

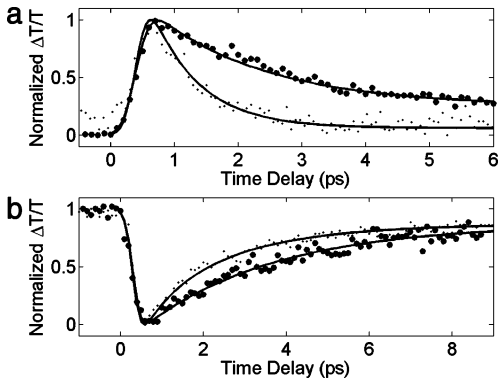

Figure 8. Oxidation effects increase the rate at which electrons and holes relax in core/shell tetrapods, as seen in relaxation from (a) high-energy state 2.44 eV or (b) near-IR transient absorption of holes in the valence band: under argon (●); after oxidation (·).

Air exposure was carefully avoided in preparing and characterizing the heterostructures, and exposure of samples to ambient air for 1 week was found to increase both the electronic and hole relaxation rates. Figure 8a shows representative traces of an increase in the relaxation of electrons in the core/shell tetrapod from 1.8 ps to 750 fs and Figure 8b a rate increase of 3.2 ps to (biexponential) 2.3 ps, 800 fs for hole relaxation in rocket tetrapods. The impact of air exposure on the luminescence of type I core/shell and especially single component semiconductor nanocrystals has received increasing attention.[24−26] Under some circumstances, air exposure can enhance luminescence efficiency, suggesting passivation of surface states,[24,25] which would be expected to decrease carrier relaxation rates. Passivation of CdSe NC's with air-saturated $CHCl_3$, for instance, has been shown to increase PL intensity by six times.[24] On the other hand, competing oxidation processes can not only create new surface defects but also gradually reduce the size of the nanocrystal through chemical conversion of surface atoms to oxides of Cd and Se. Diminishing luminescence as well as other complex behaviors has been reported in CdSe quantum dots as a function of exposure time and conditions.[26] In the samples used in this experiment, CdTe NC's have been observed to be more sensitive to oxidation than CdSe and, given the relatively long time of air exposure, the current results are consistent with the introduction of new surface defect states that facilitate rapid carrier relaxation in the heterostructures.

Tetrapod nanostructures are formed from four wurtzite nanorods extending from the (111), (11$\bar{1}$), ($\bar{1}\bar{1}$1), and ($\bar{1}$1$\bar{1}$) surfaces of a core zinc blende dot. Optical characteristics are expected to be dominated by the 40 nm long, 6 nm wide rod arms,[27] but alteration of the potential, symmetries, and hence the energy levels of the electronic states upon change in shape should affect the nature of excited carrier relaxation. Li et al. have used the method of semiempirical pseudopotentials to perform theoretical calculations of electronic states in nanostructures of different shapes.[3] In a tetrapod with arms 4.6 nm long and 2.2 nm in diameter, the lowest electronic state was calculated to be completely localized in the zinc blende core whereas the first hole state was found to reside along the arms of the tetrapod. Long

distance separation of charge could theoretically be achieved with two different crystal structures. In the case of the heterostructures, separation of charge is not only favorable because of the inherent wurtzite and zinc blende crystal structures but also would occur primarily from the type II alignment (Figure 2) at the interfaces. From the absorbance spectra (Figure 3) it is evident that the interface engenders sub-bandgap transitions further into the red than single-component tetrapods and rods.

The energy levels probed using different wavelengths of light yield monoexponential rise and biexponential decay kinetics, reminiscent of results for nanorods reported elsewhere.[18] The relaxation rates of lighter electrons were slower than that of heavier holes. However, all electronic levels of the tetrapods were found to populate and depopulate at slower rates when compared to both rods and dots. Excited electrons populate high-energy conduction band states within several hundreds of femtoseconds compared to times of <100 fs in CdSe rods. Similar slow behavior was observed in the band-edge states as well, with rocket tetrapods requiring nearly 2.1 ps to relax.

Charge-separating behavior was observed indirectly through probing the 1S excitonic transition and comparing to CdSe rods of similar dimensions. An alternate approach of exciting only the lower band-gap CdTe semiconductor was considered, which would have decoupled the bleaching responses, but the desired wavelength was not attainable with the current experimental design. The period of optical transparency reflects the existence of an exciton, and typical lifetimes in CdSe have been measured to be hundreds of picoseconds. Excitons persisted longer in the CdSe rods than in either the rocket or core/shell, as evidenced by the slower bleaching of the excitonic transition (Figure 5). Dissociation of the interacting electron and hole vacated the excitonic transition earliest in the core/shell structure, leading to the onset of decay at 4 ps. Rocket tetrapods, on the other hand, did not show a decrease in transmission until 10 ps later, and this is consistent with the larger nanorod arms that could support the excitons.

The study of tetrapod heterostructures adds both to the characterization of type II nanostructures and to the role that shape plays in relaxation dynamics. Practical use of such heterostructures in applications such as photovoltaics[28] will require the existence of efficient charge separation and transport along the nanorod arms. Absorbance and photoluminescence spectra indicate such charge separation and femtosecond pump−probe experiments provide a quantitative description of the kinetics.

Acknowledgment. This work was supported by Experimental Physical Chemistry Section of the National Science Foundation. P. Peng was supported by the IGERT foundation.

Note Added after ASAP Publication. This article was published ASAP on August 26, 2005. Additional authors have been added to the manuscript. The correct version was posted on September 1, 2005.

References

(1) Milliron, D. J.; Hughes, S. M.; Cui, Y.; Manna, L.; Li, J.; Wang, L.-W.; Alivisatos, A. P. *Nature* **2004**, *430*, 190.
(2) Kim, S.; Fisher, B.; Eisler, H. J.; Bawendi, M. G. *J. Am. Chem. Soc.* **2003**, *125*, 11466.
(3) Li, J.; Wang, L.-W. *Nano. Lett.* **2003**, *3*, 1357.
(4) Chen, C.-Y.; Cheng, C.-T.; Yu, J.-K.; Pu, S.-C.; Cheng, Y.-M.; Chou, P.-T.; Chou, Y.-H.; Chiu, H.-T. *J. Phys. Chem. B* **2004**, *108*, 10687.
(5) Balet, L. P.; Ivanov, S. A.; Piryatinski, A.; Achermann, M.; Klimov, V. I. *Nano. Lett.* **2004**, *4*, 1485.
(6) Ivanov, S. A.; Nanda, J.; Piryatinski, M. A.; Balet, L. P.; Bezel, I. V.; Ankeeva, P. O.; Tretiak, S.; Klimov, V. I. *J. Phys. Chem. B* **2004**, *108*, 10625.
(7) Little, R. B.; Burda, C.; Link, S.; Logunov, S.; El-Sayed, M. *J. Phys. Chem. A* **1998**, *102*, 6581.
(8) Braun, M.; Link, S.; Burda, C.; El-Sayed, M. *Phys. Rev. B* **2002**, *66*, 205312.
(9) Yeh, A. T.; Cerullo, G.; Banin, U.; Mews, A.; Alivisatos, A. P.; Shank, C. V. *Phys. Rev. B* **1999**, *59*, 4973.
(10) Lou, Y.; Chen, X.; Samia, A. C.; Burda, C. *J. Phys. Chem. B* **2003**, *107*, 12431.
(11) Klimov, V. I. *J. Phys. Chem. B* **2000**, *104*, 6112.
(12) Empedocles, S.; Bawendi, M. *Acc. Chem. Res.* **2004**, *32*, 389.
(13) Benisty, H.; Sotomayor-Torres, C. M.; Weisbuch, C. *Phys. Rev. B* **1991**, *44*, 10945.
(14) Efros, A. L.; Kharchenko, V. A.; Rosen, M. *Solid State Commun.* **1995**, *93*, 281.
(15) Darugar, Q.; Landes, C.; Link, S.; Schill, A.; El-Sayed, M. *Chem. Phys. Lett.* **2003**, *373*, 284.
(16) El-Sayed, M. *Acc. Chem. Res.* **2004**, *37*, 326.
(17) Yu, P.; Nedeljkovic, J. M.; Ahrenkiel, P. A.; Ellingson, R. J.; Nozik, A. J. *Nano. Lett.* **2004**, *4*, 1089.
(18) Mohamed, M. B.; Burda, C.; El-Sayed, M. *Nano. Lett.* **2001**, *1*, 589.
(19) Manna, L.; Milliron, D. J.; Meisel, A.; Scher, E. C.; Alivisatos, A. P. *Nature Mater.* **2003**, *2*, 382.
(20) Manna, L.; Scher, E. C.; Alivisatos, A. P. *J. Cluster Sci.* **2002**, *13*, 521.
(21) Yu, W.-W.; Qu, L.-H.; Guo, W.-Z.; Peng, X.-G. *Chem. Mater.* **2003**, *15*, 2854.
(22) Schill, A. W.; El-Sayed, M. *J. Phys. Chem. B* **2004**, *108*, 13619.
(23) Burda, C.; Link, S.; Mohamed, M.; El-Sayed, M. *J. Phys. Chem. B* **2001**, *105*, 12286.
(24) Myung, N.; Bae, Y.; Bard, A. J. *Nano. Lett.* **2003**, *3*, 747.
(25) Muller, J.; Lupton, J. M.; Rogach, A. L.; Feldmann, J. *Appl. Phys. Lett.* **2004**, *85*, 381.
(26) Cordero, S. R.; Carson, P. J.; Estabrook, R. A.; Strouse, G. F.; Buratto, S. K. *J. Phys. Chem. B* **2000**, *104*, 12137.
(27) Manna, L.; Scher, E. C.; Alivisatos, A. P. *J. Am. Chem. Soc.* **2000**, *122*, 12700.
(28) Sun, B.; Marx, E.; Greenham, N. C. *Nano. Lett.* **2003**, *3*, 961.

NL0511667